

## Supporting information

### **Artificial Visual Perception System Based on ZnO Threshold Switching Neurons with Integrated Rate and Time-to-first-spike Coding**

Liang Wang,<sup>1,2</sup> Le Zhang,<sup>1</sup> Shuaibin Hua,<sup>1</sup> Puli Gan,<sup>1</sup> Qiuyun Fu\*,<sup>2</sup> Xin Guo\*<sup>1</sup>

<sup>1</sup> State Key Laboratory of Material Processing and Die & Mould Technology, School of Materials Science and Engineering, Huazhong University of Science and Technology, Wuhan 430074, P. R. China

<sup>2</sup> Engineering Research Center for Functional Ceramics of Ministry of Education, School of Integrated Circuits, Huazhong University of Science and Technology, Wuhan 430074, P. R. China

\*E-mails: [xguo@hust.edu.cn](mailto:xguo@hust.edu.cn); [fuqy@mail.hust.edu.cn](mailto:fuqy@mail.hust.edu.cn)

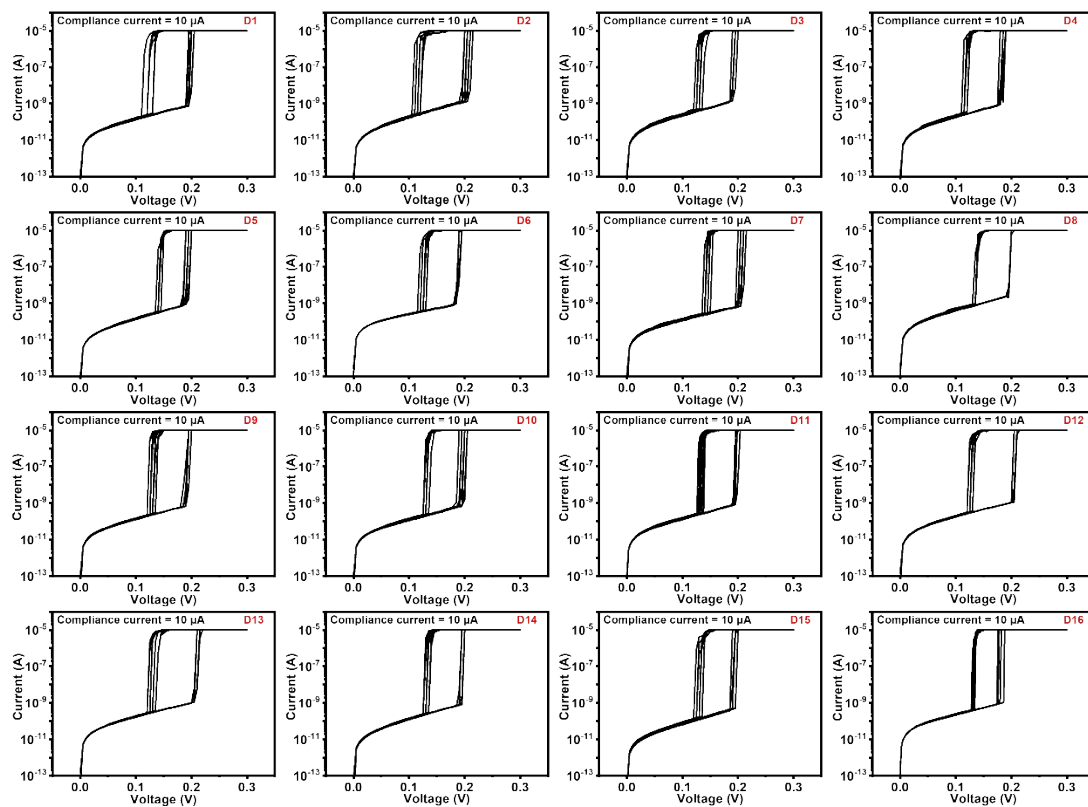


**Figure S1.** I-V characteristic curves for 16 randomly selected devices, each tested with 10 cycles of DC voltage sweeps.

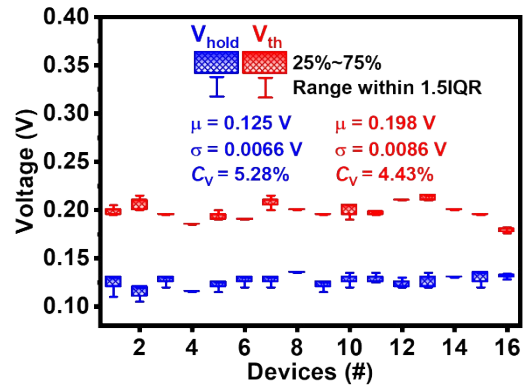


**Figure S2.** Distribution of  $V_{th}/V_{hold}$  over 10 sweeps from 16 devices. The average value ( $\mu$ ) and standard deviation ( $\sigma$ ) of  $V_{th}$  are 0.198 V and 0.0086 V, respectively, with cumulative probability variation ( $C_v$ ,  $\sigma/\mu$ ) of 4.43%. Similarly, the  $\mu$  and  $\sigma$  of  $V_{hold}$  are 0.125 V and 0.0066 V, respectively, with a  $\sigma/\mu$  ratio of 5.28%. These results demonstrate a high level of consistency between devices.

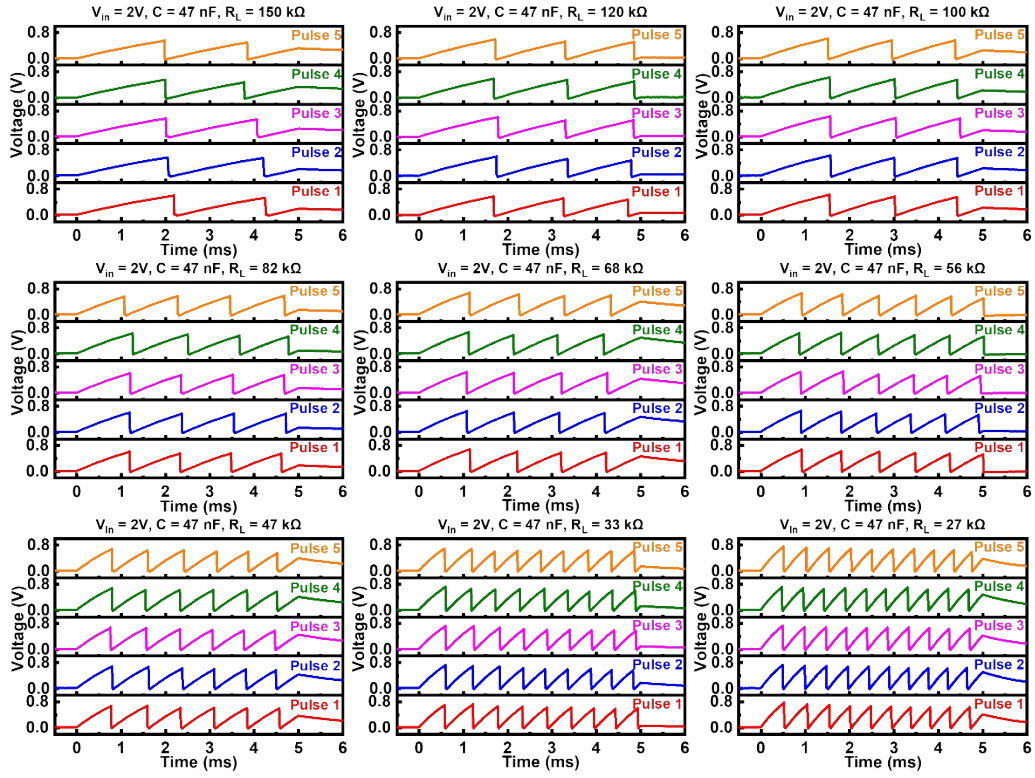


**Figure S3.** Output waveforms of the artificial ZnO neuron under varying load resistances ( $R_L$ ) ranging from 150 k $\Omega$  to 27 k $\Omega$ , with a fixed input voltage ( $V_{in} = 2$  V) and capacitance ( $C = 47$  nF). Each condition was tested five times to ensure reproducibility. The results demonstrate the effect of  $R_L$  on the spiking behavior, where the number and timing of voltage pulses are modulated by the load resistance.

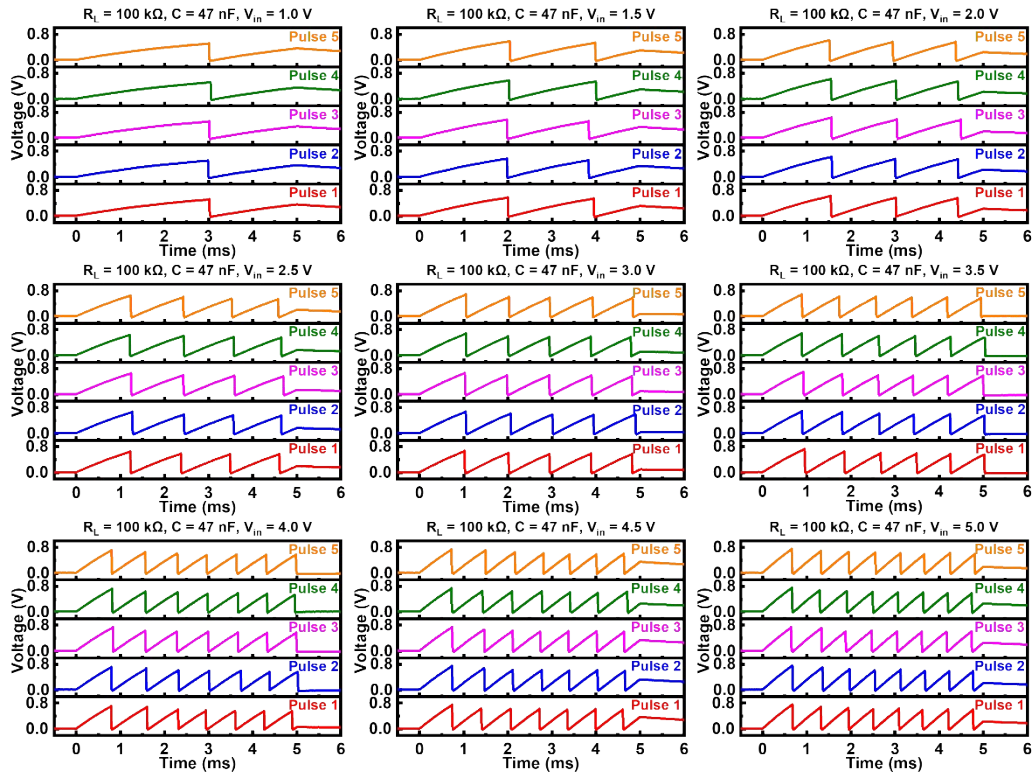


**Figure S4.** Output waveforms of the artificial ZnO neuron under varying input voltages ( $V_{in}$ ) from 1.0 V to 5.0 V, with a fixed load resistance ( $R_L = 100 \text{ k}\Omega$ ) and capacitance ( $C = 47 \text{ nF}$ ). Each condition was measured five times to confirm consistency and reliability. As the input voltage increases, the number of output voltage pulses increases, indicating a higher spiking frequency.

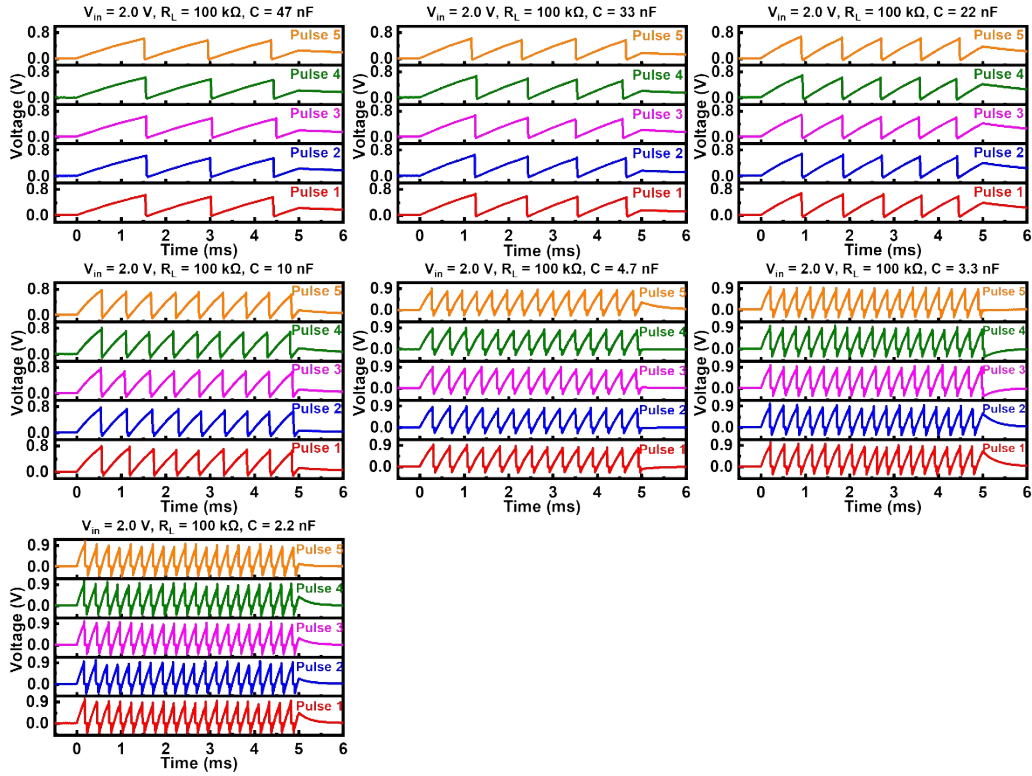


**Figure S5.** Output waveforms of the artificial neuron under varying capacitance values ranging from 47 nF to 2.2 nF, with a fixed input voltage ( $V_{in} = 2.0$  V) and load resistance ( $R_L = 100$  k $\Omega$ ). Each condition was tested five times to ensure reproducibility. The results illustrate the effect of capacitance on the spiking behavior, where a decrease in capacitance leads to an increase in the spiking frequency.

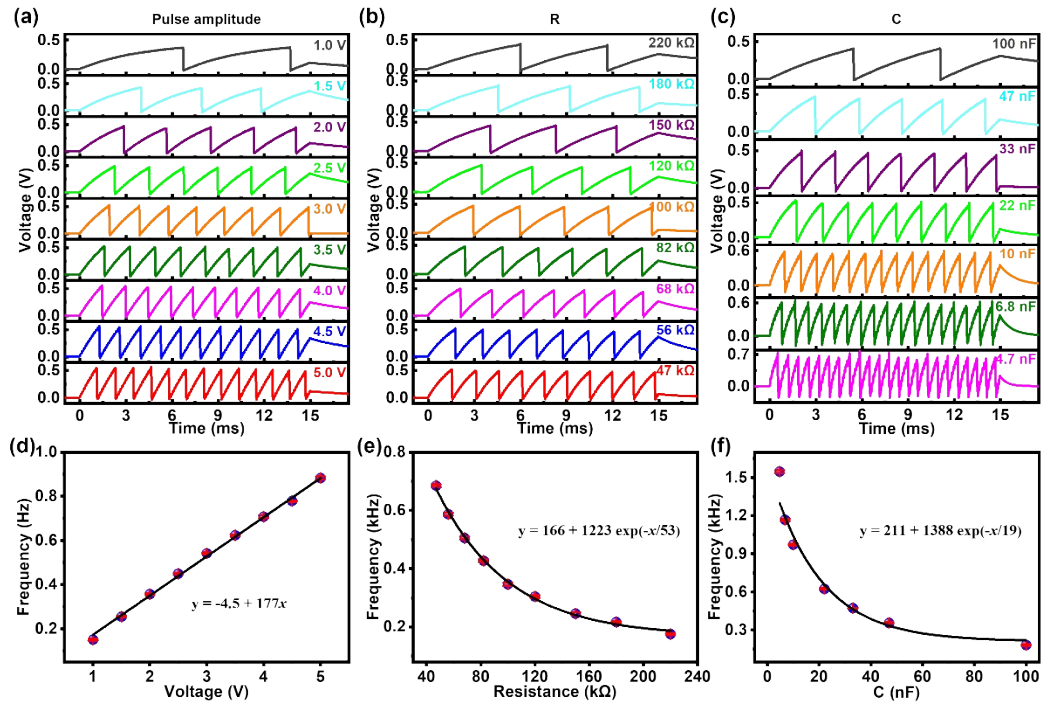


**Figure S6.** Systematic investigation of the LIF behavior of the artificial ZnO neuron. Output waveforms under varying (a) series resistance, (b) input voltage amplitude, and (c) parallel capacitance. Spiking frequency as a function of (d)  $R_L$ , (e)  $V_{in}$ , and (f)  $C$ , demonstrating tunability through external circuit parameters. The input voltage consists of a sequence of 150 pulses, each with a pulse width of 50  $\mu$ s and a 50  $\mu$ s interval between pulses.

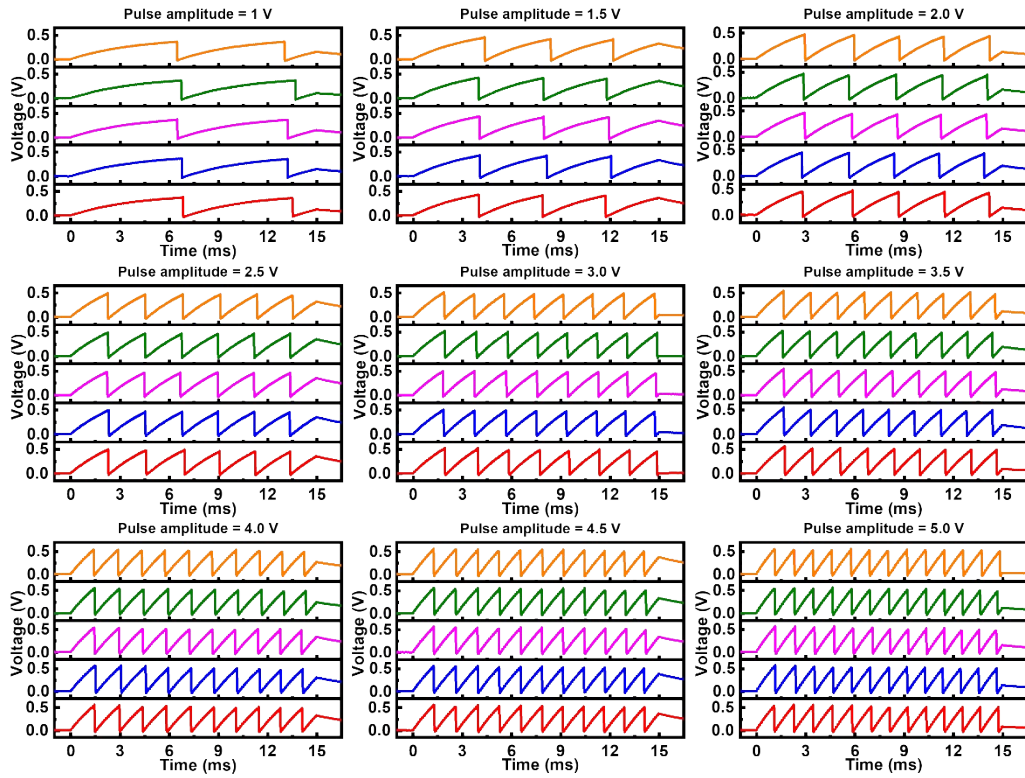


**Figure S7.** The LIF behavior of the artificial ZnO neuron under varying input pulse amplitudes. The output waveforms are shown for pulse amplitudes ranging from 1 V to 5 V, with increments of 0.5 V. For each pulse amplitude, five repeated measurements were conducted to evaluate the consistency of the LIF behavior.

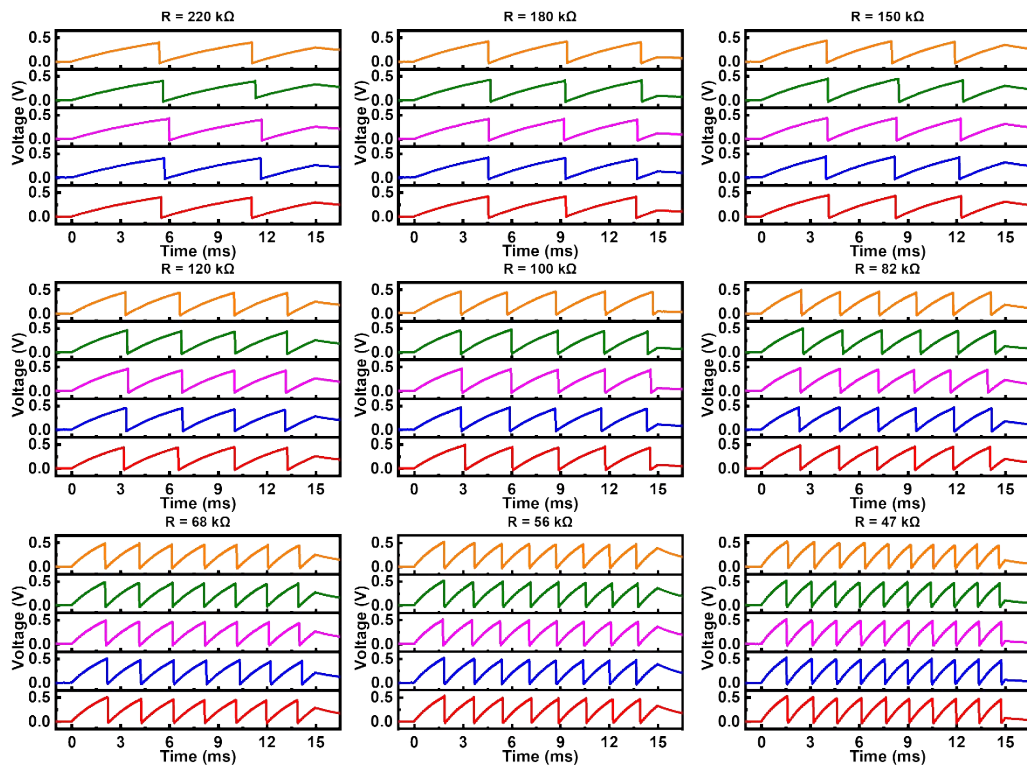


**Figure S8.** Examination of the influence of series resistance ( $R$ ) on the LIF behavior of the artificial ZnO neuron. Output waveforms are presented for a range of series resistance values ( $R = 220 \text{ k}\Omega$  to  $47 \text{ k}\Omega$ ). For each resistance value, five repeated measurements were conducted to evaluate the consistency and reproducibility of the spiking behavior.

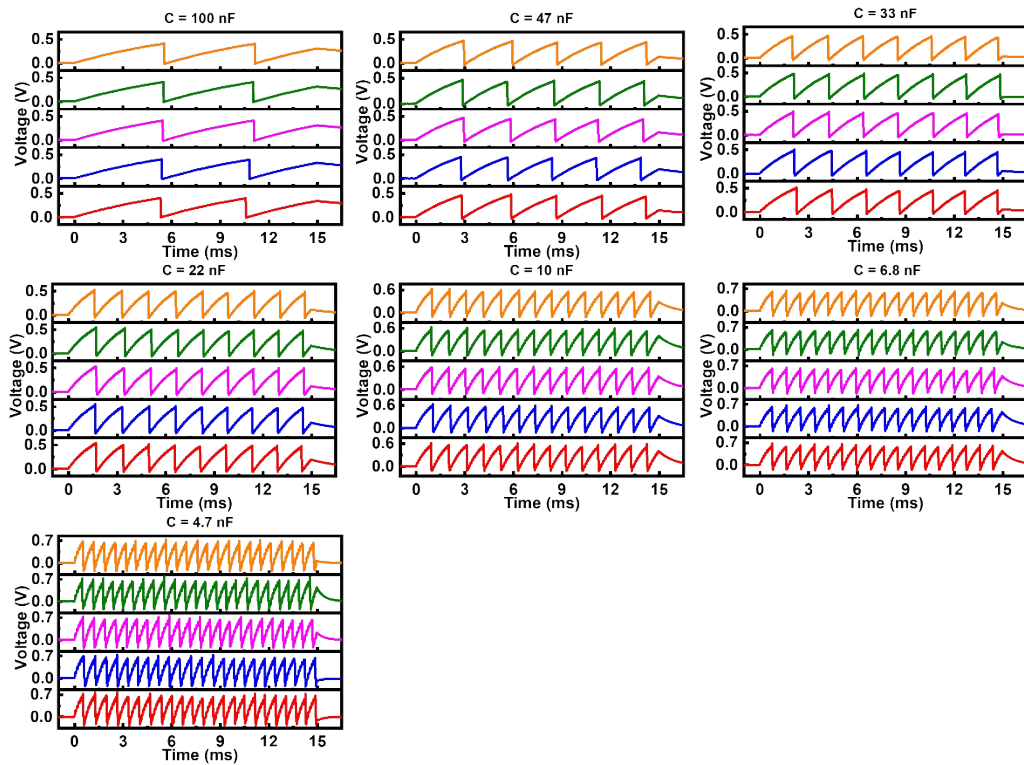


**Figure S9.** Investigation of the effect of capacitance ( $C$ ) on the spiking behavior of the artificial ZnO neuron. Output waveforms are shown for various capacitance values ranging from 100 nF to 4.7 nF. For each capacitance value, five repeated measurements were conducted to evaluate the consistency of the spiking behavior.

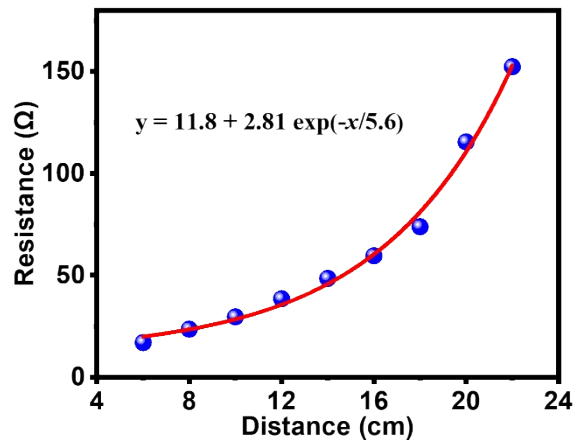


**Figure S10.** Dependence of the photoresistor's resistance on the distance between the light source and the photoresistor. The resistance increases exponentially with distance, as described by the fitted equation  $y = 11.8 + 2.81e^{(-x/5.6)}$ . Blue dots represent experimental data, and the red curve represents the fitted exponential model.

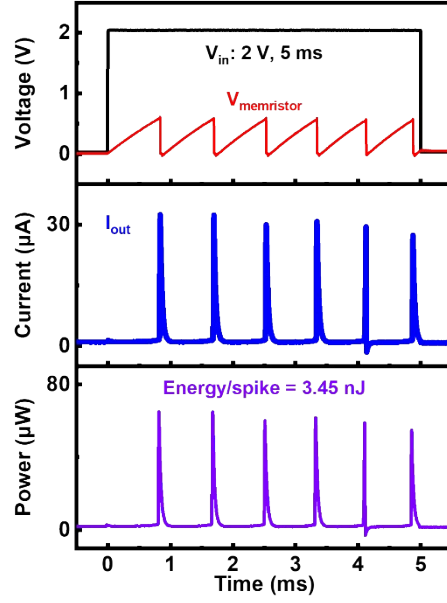


**Figure S11.** Energy consumption per oscillation spike.

**Figure S11** shows the calculated transient power ( $P_{\text{spike}}$ ) of the Ag/ZnO/Pt visual neuron as a function of time. The power is expressed as:

$$P_{\text{spike}}(t) = V_{\text{memristor}}(t) \times I_{\text{out}}(t) \quad (1)$$

where  $V_{\text{memristor}}$  and  $I_{\text{out}}$  are the transient voltage across the memristor and the output current of the artificial neuron, respectively. The energy consumption per spike ( $E_{\text{spike}}$ ) was estimated by integrating the transient power over time:

$$E_{\text{spike}} = \int P_{\text{spike}}(t) dt \quad (2)$$

In this study, the energy consumption per oscillation spike was calculated based on the oscillation data in **Figure 5b**, where the light source was positioned 16 cm from the photosensitive resistor. The integration of the transient power over the duration of each spike yielded an energy consumption of approximately 3.45 nJ per spike, as shown in **Figure S11**.

**Table S1.** Comparison with artificial neurons based on diffusive TS memristors reported in literatures.

Device structure	$V_{th}/V_{hold}$ (V)	$V_{th}$ variation	Ref.
Ag/TaO <sub>x</sub> /ITO	~0.3 / 0.1	-(1000 cycles)	1
Pt/Ag NDs/HfO <sub>2</sub> /Pt	0.607 / 0.201	4.8% (-)	2
Pt/HfO <sub>2</sub> /Ag	0.38 / 0.18	9% (100 cycles)	3
Pt/Ag/TiN/HfAlO <sub>x</sub> /Pt	0.4 / ~0	6.3% (200 cycles)	4
Ag/ZrO <sub>x</sub> /Pt	0.4 / 0.02	5.6% (50 cycles)	5
Ag/Ta <sub>2</sub> O <sub>5</sub> / HfO <sub>2</sub> /Pt	0.19 / ~0	7.3% (20 cycles)	6
Ag/ IGZO/ITO	1.69 / 0.18	12% (50 cycles)	7
Pd/HfO <sub>x</sub> /Ag	0.15 / 0.04	- (100 cycles)	8
Pt/Ag/SiO <sub>2</sub> NRs/Ag/Pt	0.5 / 0.3	-(500 cycles)	9
Au/Ag/hBN/Au/Ti	0.202 / 0.024	16.8% (500 cycles)	10
Ag/ZnO/Pt	0.179 / 0.13	1.508% (1000 cycles)	This work

**Table S2.** Comparison of threshold switching memristors for artificial neuron.

Device structure	Neuron type	Energy/spike	Ref.
Ag/TaO <sub>x</sub> /ITO	LIF	250 nJ	1
Pt/Ag/HfO <sub>2</sub> /Pt	Oscillation	1.8 μJ	11
Pt/Ag/TaO <sub>x</sub> /AlO <sub>x</sub> /ITO	Oscillation	0.3-240 nJ	12
Pt/VO <sub>2</sub> /Pt	Oscillation	100-250 μJ	13
Pt/NbO <sub>2</sub> /Pt	Oscillation	2-10 μJ	14
Pt/NbO <sub>x</sub> /TiN	Oscillation	2.1 nJ	15
Ag/ZnO/Pt	LIF & Oscillation	3.45 nJ	This work

## References

1. C. Chen, Y. He, H. Mao, L. Zhu, X. Wang, Y. Zhu, Y. Zhu, Y. Shi, C. Wan and Q. Wan, *Adv. Mater.*, 2022, **34**, 2201895.
2. Y. Li, J. Tang, B. Gao, X. Li, Y. Xi, W. Zhang, H. Qian and H. Wu, *Journal of Semiconductors*, 2021, **42**, 064101.
3. Y. Liu, W. Wang, S. He, H. Liu, Q. Chen, G. Li, J. Duan, Y. Liu, L. He, Y. Xiao, S. Yan, X. Zhu, R.-W. Li and M. Tang, *Phys. Scr.*, 2024, **99**, 045941.
4. Y. F. Lu, Y. Li, H. Li, T. Q. Wan, X. Huang, Y. H. He and X. Miao, *IEEE Electr. Device L.*, 2020, **41**, 1245-1248.
5. J.-H. Yang, S.-C. Mao, K.-T. Chen and J.-S. Chen, *Adv. Electron. Mater.*, 2023, **9**, 2201006.
6. Y.-R. Jeon, D. Akinwande and C. Choi, *Nanoscale Horizons*, 2024, **9**, 853-862.
7. W. Peng, C. Liu, C. Xu, C. Qin, N. Qin, H. Chen, T. Guo and W. Hu, *Science China Materials*, 2024, **67**, 2661-2670.
8. R. Midya, Z. Wang, J. Zhang, S. E. Savel'ev, C. Li, M. Rao, M. H. Jang, S. Joshi, H. Jiang, P. Lin, K. Norris, N. Ge, Q. Wu, M. Barnell, Z. Li, H. L. Xin, R. S. Williams, Q. Xia and J. J. Yang, *Adv. Mater.*, 2017, **29**, 1604457.
9. Y. G. Song, J. E. Kim, J. U. Kwon, S. Y. Chun, K. Soh, S. Nahm, C.-Y. Kang and J. H. Yoon, *ACS Appl. Mater. Interfaces*, 2023, **15**, 5495-5503.
10. Y. Jo, D. Y. Woo, G. Noh, E. Park, M. J. Kim, Y. W. Sung, D. K. Lee, J. Park, J. Kim, Y. Jeong, S. Lee, I. Kim, J.-K. Park, S. Park and J. Y. Kwak, *Adv. Funct. Mater.*, 2024, **34**, 2309058.
11. Q. Hua, H. Wu, B. Gao, Q. Zhang, W. Wu, Y. Li, X. Wang, W. Hu and H. Qian, *Global Challenges*, 2019, **3**, 1900015.
12. K. Shi, S. Heng, X. Wang, S. Liu, H. Cui, C. Chen, Y. Zhu, W. Xu, C. Wan and Q. Wan, *IEEE Electr. Device L.*, 2022, **43**, 2196-2199.
13. W. Yi, K. K. Tsang, S. K. Lam, X. Bai, J. A. Crowell and E. A. Flores, *Nat. Commun.*, 2018, **9**, 4661.
14. M. D. Pickett, G. Medeiros-Ribeiro and R. S. Williams, *Nat. Mater.*, 2013, **12**,

114-117.

15. J. Wen, L. Zhang, Y.-Z. Wang and X. Guo, *ACS Appl. Mater. Interfaces*, 2024, **16**, 998-1004.